Journal of Molecular Liquids 410 (2024) 125611

Contents lists available at ScienceDirect

Journal of Molecular Liquids

journal homepage: www.elsevier.com/locate/molliq

Reactivities of 4-amino salicylic acid and its 'Green' inhibition into nano sized β-cyclodextrin for Anti-Tuberculosis drug delivery

Shruti Sharma [a], Pooja Yadav [a], Meenakshi Rana [b], Papia Chowdhury [a,*]

[a] Department of Physics and Materials Science and Engineering, Jaypee Institute of Information Technology, Noida 201309, Uttar Pradesh, India
[b] Department of Physics, School of Sciences, Uttarakhand Open University, Haldwani, 263139, Uttarakhand, India

ARTICLE INFO

Keywords:
4-amino salicylic acid
Tuberculosis
DFT
Molecular docking
MD Simulation

ABSTRACT

In the present work, 4-amino salicylic acid (PAS) which is an oral antibiotic against tuberculosis is being investigated for its potential "Green" effectivity in trapped conditions within nano sized good solubilizing drug receptor. The process is totally "green" as no toxic materials, chemicals and solvent other than water has been used throughout the encapsulation /complexation process. Cyclodextrin glycosyltransferase (3CGT) and its by-product beta (β)-cyclodextrin (β-CD) usually act as nano sized good solubilizing agents for many drugs. In aqueous medium both 3CGT and β-CD can create drug: receptor complex by encapsulating the drug into its nano sized cavity and can increase the aqueous solubility of probe drug depending on the ionic strength. PAS was initially screened by its drug likeness properties by ADMET analysis. Structural analysis and chemical reactivity of PAS have been checked by density functional theory with basis set B3LYP/6-311G++*(d,p) in aqueous environment. The electronic properties (atomic charges, electrostatic potential, and uv–visible absorption & fluorescence analysis) have been studied to check the possibility of 1:1 complex formation between PAS: β-CD. To understand the type and strength of interactions between PAS and receptor, molecular docking and molecular dynamics simulations have been performed between PAS and cyclodextrin glycosyltransferase (3GGT). PAS has shown strong interaction possibilities both as 1:1 inclusion complex (PAS: β-CD) and as PAS: 3CGT complex. Our in-silico and experimental outcomes have recommended 4-amino salicylic acid's better efficacy as a promising inhibitor inside cyclodextrin nano-cavity for targeting tuberculosis.

1. Introduction

In the present day, about one-quarter of the world's population is estimated to be infected by bacterium Mycobacterium tuberculosis (MTB) [1]. Tuberculosis (TB), a severe infectious disease primarily impacting the lungs, can also target other organs like the kidneys, spine, and brain. As per WHO reports, approximately 9.9 million cases of TB were reported and 1.5 million people died globally only in 2020 [2–5]. The primary receptor for MTB is human. The infection used to spread by air droplet nuclei from infected patient. In the developing countries like India, Pakistan, Bangladesh etc., TB is one of the leading diseases which has continued to bear the heaviest burden of the worldwide TB epidemic over the past five years [6,7]. The best curative method for TB is known as directly observed treatment, short course (DOTS) which is used worldwide in tuberculosis prevention programmes, as well as elucidating the biological properties of the disease's etiologic agent [8,9]. Despite the availability of many effective drugs like: isoniazid, rifampicin, pyrazinamide and ethambutol, TB continues to cause significant morbidity and mortality, due to emergence of multidrug-resistance (MDR) and extensively drug-resistance (XDR) [10,11]. Further, programmatic failure, lack of resources have also facilitated the burgeoning of drug resistance [12]. New TB treatment regimens aimed at new chemical entities against drug-resistant TB.

Many new small sized inhibitors have shown their promising candidature as the potential drugs for shortening TB treatment in animal models [13], clinical trials [14–16]. 4-amino salicylic acid is one of such drug candidates having anti tuberculosis effect (Fig. 1a). In medical industry the brand name of this drug is PASER or PAS [17]. The tuberculostatic effect of PAS was first reported in 1943 just after its invention [18–21]. PAS was first used for the treatment of "Monaldi fistulas and abscesses" [20]. Later on, it was used for pulmonary TB situations [21]. Salicylic acid of PAS can cause an increase of oxygen consumption and carbon dioxide production by tubercle bacilli. The presence of amino group in para position and salicylic acid can inhibit the growth of

* Corresponding author.
E-mail address: papia.chowdhury@jiit.ac.in (P. Chowdhury).

https://doi.org/10.1016/j.molliq.2024.125611
Received 14 February 2024; Received in revised form 19 July 2024; Accepted 21 July 2024
Available online 22 July 2024

bacillus by causing 50 % to 75 % decrease in growth of tubercle bacilli at a concentration of 10^{-5} M [22,23]. Pas has some side effects like nausea, vomiting, diarrhoea, gastrointestinal intolerance and stomach pain, which decreases patient compliance [24]. With the rise of multidrug-resistant (MDR) strains of M. tuberculosis, PAS has emerged as a crucial second-line antitubercular drug [25,26]. Despite being a top anti-TB drug, the molecular and chemical mechanisms of PAS remain unclear, and the causes of its gastrointestinal intolerance are still undefined.

Comprehensive knowledge about any drug's molecular composition, including its chemical and biological properties, toxicity, and optical and electronic properties, is essential for assessing its effectiveness against the target disease. Additionally, reactivity descriptors help define a drug's solubility, permeability, and binding ability to its target. Density functional theory (DFT) is one of the promising ab initio computational method for providing excellent electronic, electrical, and reactivity descriptors of diverse organic/inorganic probe compounds [27,28]. For any orally consumable drug in liquid form, the problem regarding the solubility and permeability could be addressed if the drug is used in its nano sized dimension which is only possible by trapping the probe drug inside nano sized good solubilizing receptor enzyme like Cyclodextrin glycosyltransferases (3CGT) (Fig. 1b) or its by-product beta (β)-cyclodextrin (β-CD) (Fig. 1c) [29]. Cyclodextrin glycosyltransferases are α amylase family of bacterial extracellular enzymes that have the unique ability to produce cyclodextrins (α(1->4) linked circular oligoglucosides) from starch. β-CD is one of the cyclic derivative of cyclodextrin glycosyltransferase having 7 glucose units linked end to end via α-1,4 linkages. In aqueous medium both 3CGT and β-CD can create receptor: inhibitor (drug) complexation by encapsulating the drug into its nano sized cavity and can increase the aqueous solubility of probe drug depending on the ionic strength. The size/shape relationship, number of hydrogen and hydrophobic interactions are some vital parameters for the stability of receptor: inhibitor complex which can easily modify the physical and chemical properties of the inhibitor molecule mostly in terms of solubility, bioavailability, toxicity etc. Receptor: drug complexation can also decrease the gastrointestinal intolerance effect of the guest drug. To fight against microbial resistance, especially for tuberculosis, a new therapeutic tool as "Green" nano approach has already been under consideration as an effective approach. For TB exposed mice, the known anti TB drug "Ethionamide" trapped within nano cavity of β-CD has already shown significant decrease of the micro bacterial burden in lungs of active TB patients [30]. It is already a reported fact that in nanosized inclusion complex form, drugs can act perfectly in terms of their solubility, stability, toxicity and antibacterial activity [31]. Drug: β-CD complex can allow higher dosing into the body part like lung, by increasing drug's solubility [32,33]. Many research works have reported that solubility, stability, and antibacterial activity of the drug: CD inclusion complex formed by individual or combined drugs [33]. Individual administration of CD nanoparticles also has shown to have the anti-mycobacterial activity as it can disrupt cell

Compound Name	Structure
(a) 4-amino salicylic acid ($C_7H_7NO_3$)	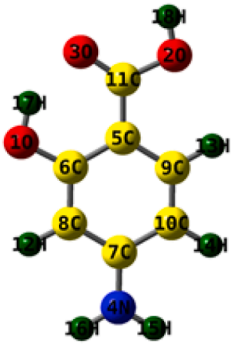
(b) Target Protein: 3CGT	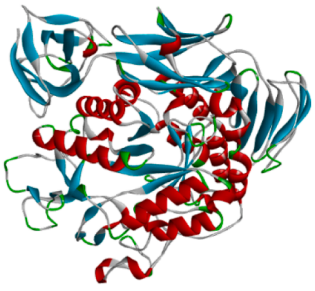
(c) (β)-cyclodextrin (β-CD)	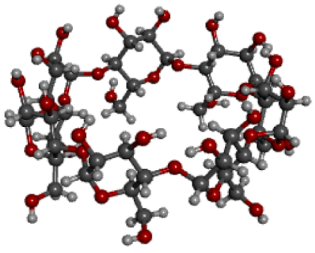

Fig. 1. (a) 4-amino salicylic acid (Obtained from Gaussian software), Receptor morphology (3CGT) (Obtained from Protein data bank), and (c) (β)-cyclodextrin (β-CD) (Obtained from Protein data bank).

surface lipid rafts and so easily respond to bacterial receptor cell invasion [34]. So, nanotechnology can help to reduce administered dose by targeting more efficiently towards infected macro-phages similarly as generated by the first line reference drug Isoniazid [35]. The process is totally "green" as no toxic materials, chemicals and solvent other than water has been used throughout the encapsulation /complexation process. Research reports suggest that unloaded poly β-CD has no impact on normal bacterial pulmonary pathogens whereas it can easily create impact on M.TB [36]. β-CD has low nephrotoxicity so can be used orally. β-CD is the most commonly used CD in pharmaceutical formulations. For the present study we have chosen both raw cyclodextrin glycosyltransferase enzyme (3CGT) and its product derivative β-CD as receptors to check the effective reactiveness, selectivity of proposed inhibitor 4-amino Salicylic Acid (PAS) as Anti-Tuberculosis Drug. The electronic properties (atomic charges, electrostatic potential, and uv–visible absorption &fluorescence analysis) have been studied to check the possibility of 1:1 complex formation between PAS: β-CD. To understand the type and strength of interactions between PAS and receptor, molecular docking and molecular dynamics simulations have been performed between PAS and 3GGT. We believe that the present work will help to understand the mechanism of action of PAS in presence of nano-sized drug carrier.

2. Materials and methods

2.1. Potential inhibitor 4-amino salicylic acid (PAS) and its preparation

PAS is a drug ($C_7H_7NO_3$), which is used as an antibiotic against the TB virus. In 1944, PAS was discovered, but it's in vitro and in vivo activity against TB was demonstrated in 1947 [18]. PAS is utilized as a backup system. antimycobacterial agent generally reserved for treatment of MDR and XDR TB [37]. Before testing the drug's structural, chemical and optical characteristics and also its ability of inhibition mechanism, solubility, permeability, gastrointestinal intolerance, we have done the virtual screening by "SWISS ADME software" (https://www.swissadme.ch) and "ADMET" (https://vnnadmet.bhsai.org/). For preliminary virtual drug screening, drug-likeness rules such as Lipinski's rule of five (Ro5), Ghose filter, Veber's rule, MDDR-like rule, Muegge rule, and others are used [38,39]. The drug in 'SDF' format is downloaded directly from PubChem (https://pubchem.ncbi.nlm.nih.gov/) and for drug preparation the drug is converted to 'PDB' format by using Auto Dock tools (https://vina.scripps.edu/) [40]. The Gauss view 05 [41], Gaussian 09 software's [42] are used to creation of molecular structure of drug and to optimized the drug's molecular structure. A common 6-311G++*(d,p) basis set was employed using the method B3LYP for optimization [43,44].

2.2. Potential target Macromolecular enzyme structure and preparation of inhibitor

In the present work, we have used Cyclodextrin Glycosyltransferase, a α amylase family of bacterial extracellular enzyme that have the unique ability to produce β-CD from degraded starch by intramolecular transglycosylation (3CGT) as the target enzyme structure. 3CGT is an enzymatically produced cyclic derivative of starch made from partially hydrolysed starch (maltodextrin). Seven alpha-(1->4) connected D-glucopyranose units make up its structure (Fig. 1). The 3CGT's 3D structure is obtained from the Protein Data Bank (https://www.rcsb.org). The water molecules existing in the structure are deleted (Fig. 1). By using the Discovery studio 2020 ((https://discover.3ds.com/discovery-studio-visualizer-download).), we have added polar hydrogen in the β-CD structure and the extracted inbuilt ligand from it. Then for further analysis the output of the β-CD structure is saved in PDB format by using AutoDock and MGL software [40].

2.3. Computational method for structural analysis

The optimization of ground and excited structures of 4-amino salicylic acid have been carried out using the Gaussian 09 program [42]. The ground state calculation was done with density functional theory (DFT) using B3LYP correlation functional having 6-311G++*(d,p) basis set [43,44]. While excited states calculation of molecule was performed using TD-DFT. The Frontier molecular orbitals (FMOs) are simulated for the PAS using Koopman's theorem [45]. Other quantum mechanical calculations, such as atomic charges (Mulliken and natural) and molecular electrostatic potential (MEP) surface mapping with electrostatic potential surface, are produced by employing the optimized structure.

2.4. Molecular docking and molecular dynamics (MD) simulation

To investigate the interaction between target β-CD and inhibitor PAS, we have used AutoDock 4.2 [40]. Molecular Graphics Laboratory (MGL) tools are used to prepare target and inhibitor structures for molecular docking. Molecular docking is a computational tool for calculating the binding energy of an inhibitor: target complex structure in its optimized form. The LINUX-based platform "GROMACS 5.1 Package [46] with GROMOS43A2 force fields [47] is used for MD simulation to calculate various thermodynamical parameters and binding energy of the inhibitor: target complex structure. Different thermodynamic parameters [Potential energy (E_{pot}), temperature (T), density (D), radius of gyration (Rg), root-mean-square deviation (RMSD), root-mean-square fluctuation (RMSF), solvent-accessible surface area (SASA), H-bonds, and interaction energies (G_{bind})] are the computed by using MD simulation. According to the MD simulation protocol, TIP3P water model was used for simulation, and 6Na + ions were applied to preserve the neutrality of the inhibitor: target complex structure.

The MMPBSA (Molecular Mechanics Poisson-Boltzmann Surface Area) approach [48] is obtained from the Adaptive Poisson-Boltzmann Solver (APBS) and GROMACS packages are used to determine the interaction free energies for the PAS: β-CD complex structure (ΔG_{bind}). After the MD simulation of the complex using the single trajectory approach is finished, ΔG_{bind} computation typically starts. For protein and ligand complex ΔG_{bind} can be written using the following equations as:

$$\Delta G_{bind,aqu} = \Delta H - T\Delta S \approx \Delta E_{MM} + \Delta G_{bind,solv} - T\Delta S \quad (1)$$

$$\Delta E_{MM} = \Delta E_{covalent} + \Delta E_{electrostatic} + \Delta E_{VanderWaals} \quad (2)$$

$$\Delta E_{covalent} = \Delta E_{bond} + \Delta E_{angle} + \Delta E_{torsion} \quad (3)$$

$$\Delta G_{bind,solv} = \Delta G_{polar} + \Delta G_{nonpolar} \quad (4)$$

where binding causes a change in −TS conformational energy, as well as changes in solvation free energy, molecular mechanical energy in the gas phase, covalent energy, electrostatic energy, and Van der Waals energy changes. Covalent energy is the sum of polar and nonpolar contributions, is the sum of bond, angle, and torsion.

2.5. Computational details

For MD simulations and associated energy calculations, a single system with an HP Intel Core i5 – 1035G1 CPU, 8 GB of RAM, Intel UHD Graphics, and a 512 GB SSD has been employed.

3. Results and discussion

3.1. Optimized structure

The most stable PAS structure in the ground state was optimised using B3LYP/6-311G++*(d,p) level of theory (Fig. 1b). Table 1 shows

Table 1
Optimized parameter of PAS.

Bond	Bond length(Å)	Bond	Bond angle (°)
O1-H17	0.97	H17- O1-C6	109.35
O1-C6	1.35	O1-C6-C5	124.12
C6- C 8	1.39	O1-C6-C8	115.78
C5- C6	1.41	C5-C6-C8	120.09
C5- C11	1.46	C6-C8-H12	117.90
C5- C9	1.41	H12-C8-C7	120.89
C5- C11	1.46	C8-C7-N4	120.70
C11-O3	1.38	C7-N4-H16	121.85
C11-O2	1.20	C7-N4-H15	120.93
O3-H18	0.96	C7-C10-H14	119.12
C9-H13	1.03	H14-C10-C9	120.47
C9-C10	1.37	C10-C9-H13	120.27
C10-H14	1.08	C10-C9-C5	122.38
C10-C7	1.41	C9-C5-C6	117.67
C7-N4	1.37	C9-C5-C11	116.93
N4-H15	1.00	C5-C11-O2	126.84
N4-H16	1.00	C5-C11-O3	113.43
C7-C8	1.39	C11-O3-H18	107.04
C8-H12	1.08	C6-C5-C11	125.39

the different bond lengths (Å) and bond angles (°) of PAS. The optimized structure of PAS shows a non-planar geometry with ground state electronic energy as −346122.675 kcal/mol. PAS possess C1 point group symmetry, which creates a high value of dipole moment of 5.23 Debye. The high dipole moment value could boost the probe system's bioactivity [49], this is a characteristic of a medicine that makes it easier for the drug and target to create a complex.

3.2. Charge analysis

Mulliken and natural charges of a system are important factors in forecasting a molecule's nucleophilic and electrophilic reactive regions. PAS comprises electron donor and acceptor groups, any target structure can be a part of a complex formed by PAS. Fig. 2 depicts different Mulliken and natural charges computed for the PAS compound. Mulliken and natural charges for the PAS compound shows almost similar results except some cases. According to the observed charge analysis, all the oxygen atoms have negative charges. O2 and O3 atoms have more negative charges (NBO: −0.6107e and Mulliken: −0.34077e) and (NBO: −0.74769e and Mulliken: −0.34083e) than O1 atom (NBO: −0.67668 e and Mulliken: −0.30067 e) (Supporting Document, SD 1, Fig. 2). All of the hydrogen atoms have positive charges. It is observed that H17 and H18 atoms have the highest positive charges than other hydrogen atoms. Higher positive charges with H17 and H18 are due to their attachment to electron-withdrawing oxygen groups. Carbon atoms in the PAS possess both positive and negative charges. C5 atom possess the maximum positive Mulliken charge of 1.101165e (SD 1, Fig. 2). While C6 atom possess the maximum negative Mulliken charge of −1.1973e. N4 atom has the negative charge (NBO: −0.77489 e and Mulliken: −0.42294 e) (SD 1, Fig. 2). The probe molecule's versatile charge variations reflect the molecule's strong ability to accept/donate electrons, and hence the system's higher reactiveness toward charges. As PAS has both electron donor and acceptor groups, it establishes its strong candidature to make complex structure with target systems.

3.3. Frontier molecular orbital (FMO) analysis

Investigation of highest occupied molecular orbital (HOMO) and lowest unoccupied molecular orbital (LUMO) are very much helpful in defining the chemical stability or reactivity, and other associated electronic or chemical properties of probe molecules [50]. The electronic energy gap (E_g) is the difference in energy between the HOMO and LUMO orbitals of the probe molecule. The computed E_{HOMO} and E_{LUMO} orbitals energies are shown in the Table 2.

In the context of Koopmans' theorem, the following equations can be used to compute various FMO-related molecular properties using the E_{HOMO} and E_{LUMO}:

$$IP = -E_{HOMO} \tag{5}$$

$$EA = -E_{LUMO} \tag{6}$$

$$\eta = \frac{E_{LUMO} - E_{HOMO}}{2}, S = \frac{1}{\eta} \tag{7}$$

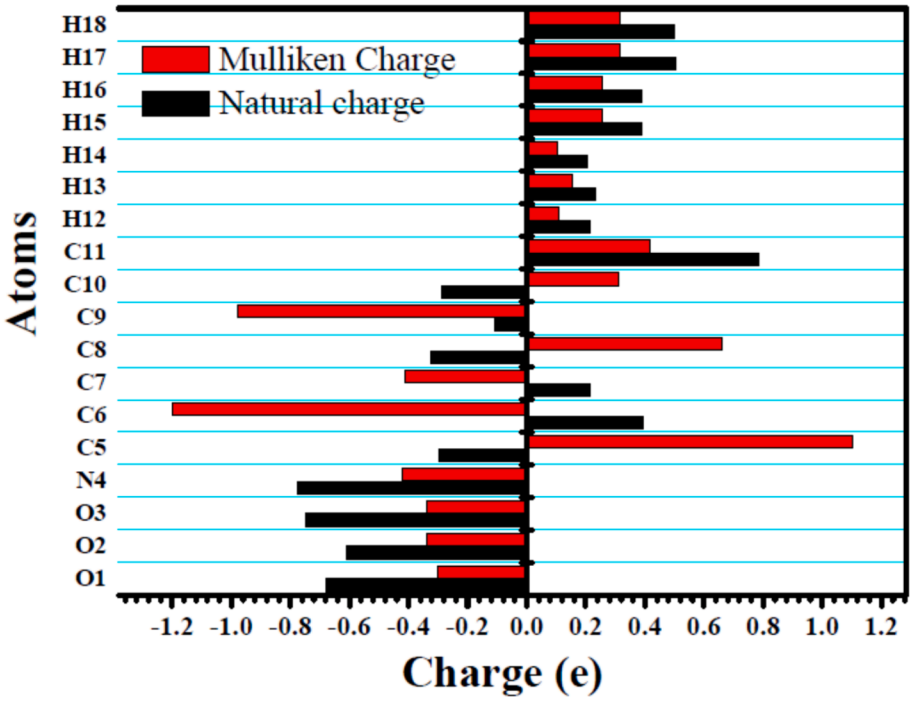

Fig. 2. Mulliken and natural charges distribution of the PAS.

Table 2
The calculated electronic properties of the PAS (all values are in eV and S is in eV^{-1}).

S.No.	Molecular Properties	Values
1.	HOMO energy	−6.128
2.	LUMO energy	−1.314
3.	Energy gap (E_g)	4.814
4.	Ionization potential (IP)	6.128
5.	Electron affinity (EA)	1.314
6.	Chemical Potential (μ)	−3.721
7.	Electronegativity (χ)	3.721
8.	Electrophilicity Index (ω)	2.860
9.	Softness (S)	0.415
10.	Hardness (η)	2.407

$$\mu = \frac{E_{HOMO} + E_{LUMO}}{2} \tag{8}$$

$$\chi = \frac{(IP + EA)}{2} \tag{9}$$

$$\omega = \frac{u^2}{2\eta} \tag{10}$$

The computed value of band gap (E_g) for PAS is observed as 4.814 eV (Table 2). A moderate value of E_g, indicates good chemical reactiveness and positive optically polarizable nature of PAS. The electron affinity (EA) is calculated as $-E_{LUMO}$, while the ionisation potential (IP) is calculated as $-E_{HOMO}$. IP and EA, are useful in evaluating the electronegativity (χ), hardness (η) and electrophilicity Index (ω), which are useful in determining the molecule's reactivity and intramolecular charge transfer capability within the molecule or towards its neighbouring environment For our probe system, high value of IP (6.128 eV) and χ (3.721 eV) confirms the higher reactivity of PAS towards other medium. Normally on the basis of ω, probe system's reactivity parameter can be categorised. It is a mild electrophile if its value is less than 0.8 eV, a moderate electrophile if it is between 0.8 and 1.5 eV, and a heavy electrophile if it is beyond 1.5 eV. In the present case the PAS has a high value of ω as 2.860 eV, indicating its high electrophile existence. The higher value of chemical potential (μ) of −3.721 eV also indicates PAS as a strong electron-withdrawing agent [51]. Chemical hardness (η) is defined as the difference between ionisation energy and electron affinity that measures the system's tolerance throughout the changing of its electronic distribution. It explains the molecule's resistance to deformation following a chemical reaction. Higher values of $\eta > 2$ can be interpreted as good chemical stability. PAS has shown the value of η as 2.407 eV which shows its restriction towards charge transfer by opposing the change in electron density distribution, or reduction in polarizability within the system. In contrast to η, the chemical softness (S) appeared to show its opposite nature (0.415 eV-1) than η. S is utilized to demonstrate the molecule's chemical reactivity [52]. Lower the value of S, higher is the chemical stability of probe system as molecule with low value of S cannot be easily deformed or get dissociated without proper perturbation like environmental effect.

We have also viewed the gross population of HOMO–LUMO molecular orbitals for PAS (Fig. 3). In PAS, the local shifts and uniform distribution of the orbitals across the geometries make up the system (Fig. 3). Within the functional groups, the orbitals in PAS appeared to change. The green surface appears to take the place of the red one, and vice versa. This further supports PAS's chemical reactivity by demonstrating that charge transfer took place between the atoms of the relevant amine, hydroxyl, and acid groups. All the FMO related parameters and HOMO–LUMO molecular orbitals pointed PAS's higher reactivity towards its target environment.

3.4. Molecular electrostatic potential (MEP) analysis

MEP is the constant electrostatic potential surface map of the probe system. The MEP surface is used to identify the molecule's electrophilic and nucleophilic reactive sites. The various colours in the MEP depict the various electrostatic potential areas, such as red colour indicates electron-rich sites, orange colour indicates partly negative charge, yellow colour indicates marginally electron-rich areas and blue colour indicates positive charge. Red, orange, yellow and blue colour in MEP represents the reactive site of the probe system while green colour in the surface indicates neutral site which does not take part in the chemical reaction. MEP surface of PAS is shown in the Fig. 4. Red colour in the MEP surface of PAS shows electron rich regions over the O2 atom, which shows the oxygen atom's lone pair of electrons in O2. Yellow colour around O1 represents marginally electron-rich area. The electrophilic areas, which are also known as electron-poor areas, are shown by the blue colour of hydrogen atoms such as H17, H18, H15 and H16. The zero potential or neutral regions are shown at the centre of the PAS. Both electrophilic and nucleophilic areas are present within PAS structure demonstrates the possibility of favourable chemical reactions between PAS and its neighbouring target environment.

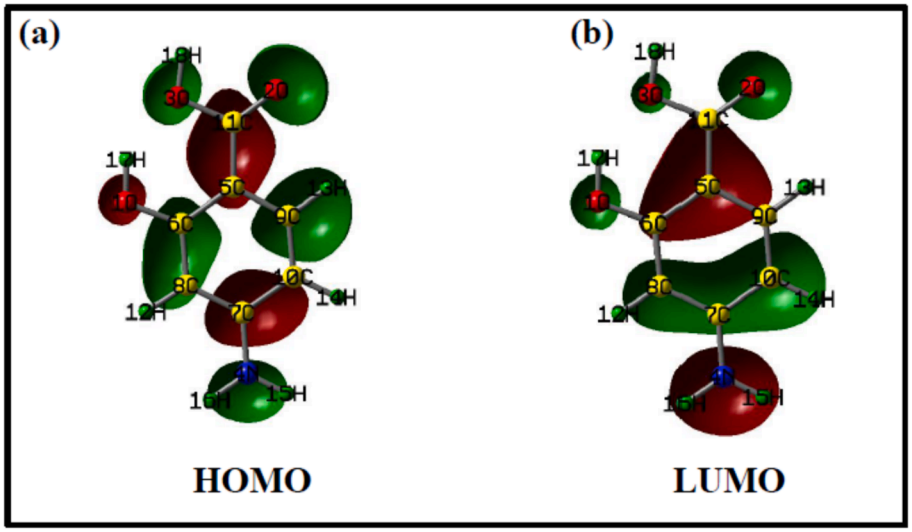

Fig. 3. HOMO, LUMO of molecular orbitals for PAS molecule.

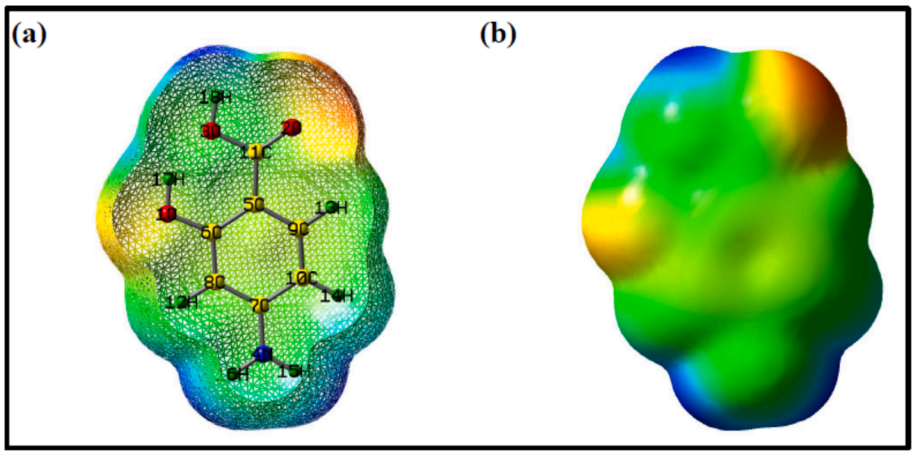

Fig. 4. Molecular electrostatic potential map of the molecule PAS.

3.5. Drug-Likely properties of PAS

We have also done the virtual screening our probe PAS as a probable drug. Drug-Likely Properties of PAS includes some necessary parameters (structural, chemical characteristics, inhibition mechanism protocols, solubility, permeability, gastrointestinal intolerance etc) and drug-likeness rules (Lipinski's rule of five (Ro5), Ghose filter, Veber's rule, MDDR-like rule, Muegge rule etc) for a proposed drug. All of these mentioned parameters and validity of rules have been computed by Auto Dock tools (https://vina.scripps.edu/), Gauss view 05, Gaussian 09, "SWISS ADME" (https://www.swissadme.ch) and "ADMET" (https://vnnadmet.bhsai.org/) softwares. For verifying drug likeness properties a rule of thumb or 'Ro5' plays an important role. Molecular weight less than 500, H-bond acceptor less than 10, H-bond donor less than 5, Moriguchi octanol–water partition coefficient (MLOGP) less than 4, and molar refractivity between 30 and 140 are the filters for Ro5 (Table 3). The Ro5-following medicines that have the necessary pharmacological characteristics can be considered as prospective candidates for vocally active medications in humans [53]. PAS follows all potential rules and lipophilicity index perfectly. PAS also follows other required rules such as; Veber, Ghose, Egan and Violate etc. (Table 3). From the ADMET analysis, we observed that PAS has good bioavailability, solubility. There is no cytotoxicity associated with it, and a daily intake of 4405 mg is the highest recommended amount.

Table 3
Physical and chemical, drug-like, lipophilic, water-soluble, and pharmacokinetic characteristics, as well as medicinal chemistry and PAS toxicity.

PAS			
Physiochemical Properties		**Water Solubility**	
Molecular Formula	$C_7H_7NO_3$	**Log *S* (SILICOS-IT)**	−0.82
Molecular Weight	153.14 g/mol	**class**	Soluble
Hydrogen Bond Donor	3	**Solubility**	2.31e + 01 mg/ml; 1.51e-01 mol/l
Hydrogen Bond Acceptor	3	**Pharmacokinetics**	
Topological Polar Surface Area	83.55 Å^2	**Gastrointestinal absorption**	High
Molar Refractivity	39.83	**BBB permeant**	No
Lipophilicity		**P-gp substrate**	No
Log $P_{o/w}$ (iLOGP)	0.84	**CYP1A2 inhibitor**	No
Log $P_{o/w}$ (XLOGP3)	1.32	**CP2C19 inhibitor**	No
Log $P_{o/w}$ (WLOGP)	0.68	**Log K_p (skin permeation)**	−6.30 cm/s
Log $P_{o/w}$ (MLOGP)	−0.70	**Drug Likeness**	
Log $P_{o/w}$ (SILICOS-IT)	0.02	**Lipinski Rule**	Yes; 0 violation
Consensus Log $P_{o/w}$	0.43	**Ghose Filter**	No; 3 violations: MW<160, MR<40, #atoms < 20
Medicinal Chemistry		**Veber (GSK) Rule**	Yes
PAINS (Pan Assey Interference Structures)	0 alert	**Egan (phatmacial) Filter**	Yes
Brenk	1 alert: aniline	**Muegge (Bayer) Filter**	No; 1 violation: MW<200
Leadlikeness	No; 1 violation: MW<250	**Bioavailability (Abbott) Score**	0.56
Toxicity			
Cyto-toxicity		No	
MRTD(mg/day)		4405	

3.6. Absorption analysis

The electrical structure and reactivity of materials determine their optical characteristics. Fig. 5 shows the computed UV–Vis spectrum of PAS molecule in water environment and Table 4 shows the measured absorption excitation energies (E) and oscillator strength (*f*). The most intense peaks for PAS molecule are observed at 285.53 nm with *f* is 0.4543 for the $S_0 \rightarrow S_1$ transition. $S_0 \rightarrow S_1$ transition has the main contribution for the formation of strong absorption band. A weak absorption is observed for $S_0 \rightarrow S_2$ transition at 274.49 nm with *f* value as 0.0863. A moderate absorption is also observed for $S_0 \rightarrow S_3$ transition at 243.79 nm with *f* value of 0.1713. Computed spectrum is obtained from single PAS, so possibility of intermolecular effect is not observable in simulated absorption data. New strong and wide redshifted absorption bands of PAS are observed between 300–380 nm in its aqueous phase experimentally [54]. Appearance of absorption peaks at higher wavelength side indicate the possibility of intermolecular interactions between PAS and external environment.

To check the possibility of intermolecular interactions of PAS in presence of nano-sized environment, we have used beta-cyclodextrin (β-CD) as the nano sized target environment. T o identify the possibility of formation of intermolecular inclusion complex between PAS and β-CD (PAS: β-CD), the binding of affinity of the PAS with target nano sized β-CD environment have been checked experimentally by steady state uv–vis absorption and fluorescence analysis from pure apo PAS and from PAS in presence of increasing concentration of β-CD in aqueous environment. The binding affinity of PAS towards β-CD has been verified by the calculation of equilibrium constant (K) by using Benesi-Hildebrand equation with experimental data. Presence of carboxylic group (–COOH) as a supporting functional group attached with

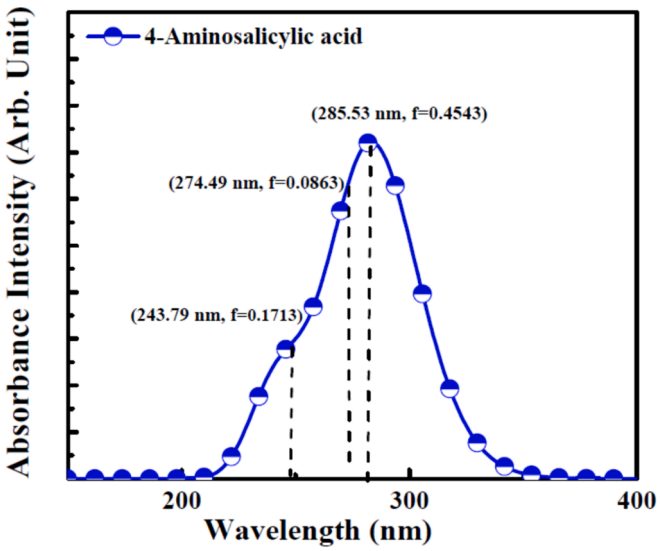

Fig. 5. Computed UV–visible spectra of PAS molecule.

Table 4
UV–visible absorption data of PAS molecule.

Absorption	Theoretical Transition	λ (nm)	E (eV)	(f)
	$S_0 \rightarrow S_1$	285.53	4.3423	0.4543
	$S_0 \rightarrow S_2$	274.49	4.5168	0.0863
	$S_0 \rightarrow S_3$	243.79	5.0857	0.1713

PAS, has been created a favourable condition to initiate intermolecular interaction with the external environment. In presence of increased concentration of β-CD, PAS shows a negligible decrement in the absorption intensity with no shift in the band position (Fig. 6). Decrement in the absorbance in presence of β-CD may be due to intermolecular interaction between PAS and β-CD with the formation of PAS: β-CD complex. Appearance of lower wavelength band around ~ 300 nm may appear due to π → π* transition due to the formation of PAS: β-CD complex. Higher wavelength absorbance around ~ 380 nm may appear due to n → π* transition from nonbonded oxygens of carboxylic groups of PAS.

The emission spectra of pure PAS, and in presence of increasing concentration of β-CD have been shown in the Fig. 7. By exciting the molecule at 290 nm Pure PAS shows dual emission bands. At 415 nm, the intensity of the higher energy emission band is stronger than that of the lower energy emission band, which is weaker at 490 nm. An increased concentration of β-CD (keeping the concentration of PAS fixed) the lower energy peak intensity at ~ 490 nm has shown an increment with the decrement in the higher energy peak intensity at ~ 415 nm which includes an *iso*-emissive point at 445 nm. In presence of β-CD both the emission peak intensities of PAS are observed to be increased or decreased without any shift in the band positions. Presence of *iso*-emissive point at 445 nm indicates the formation of new type complex between PAS and β-CD in aqueous environment. The geometrical representation of β-CD and PAS: β-CD complex is shown in the Fig. 8. To verify what type of PAS: β-CD complex formation and corresponding equilibrium, we have used Bensai-Hildebrand plot followed by Equation (11). The Benesi-Hildebrand method is a mathematical technique that is used to calculate the equilibrium constant K and the stoichiometry of non-bonding interactions [55].

$$\frac{1}{I - I_0} = \frac{1}{K(I_1 - I_0)[X^{n+}]} + \frac{1}{(I_1 - I_0)} \tag{11}$$

where I_0 is the emission intensity of apo PAS, I_1 represents the emission intensity of PAS in presence of maximum concentration of β-CD (20 mM). I is the fluorescence intensity of PAS in presence of variable β-CD concentrations (10 mM to 19 mM). The Bensai-Hildebrand plot is appeared to be straight line which validated 1:1 complexation between PAS and β-CD (Fig. 9) with an equilibrium association constant (K) value 4.8 x 10^3 M^{-1}.

3.7. Analysis of molecular docking result

After checking the possibility of complexation between PAS and β-CD through absorption and emission data, molecular docking of PAS with the parent cyclodextrin glycosyltranferases receptor 3CGT were performed to validate the formation PAS: 3CGT complex further by Vina Auto Dock. The outcomes of the molecular docking were examined using Discovery Studio Visualizer software [56]. All the poses for PAS with their binding energy, dreiding energy, dipole moment, number of hydrogen bonded and electrostatic interactions and inhibition constant has shown in SD 2. The basis of the best pose selection is the number of hydrogen bonded and hydrophobic interactions, binding energy, dreiding energy and lowest inhibition constant value of the complex at

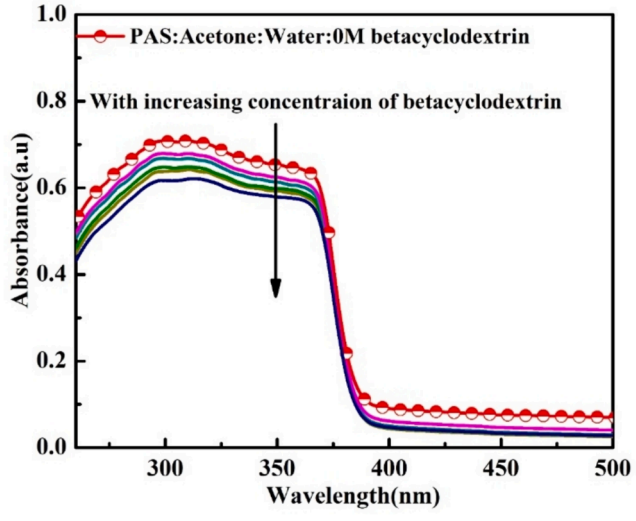

Fig. 6. Absorption spectra of apo PAS in aqueous solution phase and PAS with increasing concentration of target β-CD (10 mM to 20 mM).

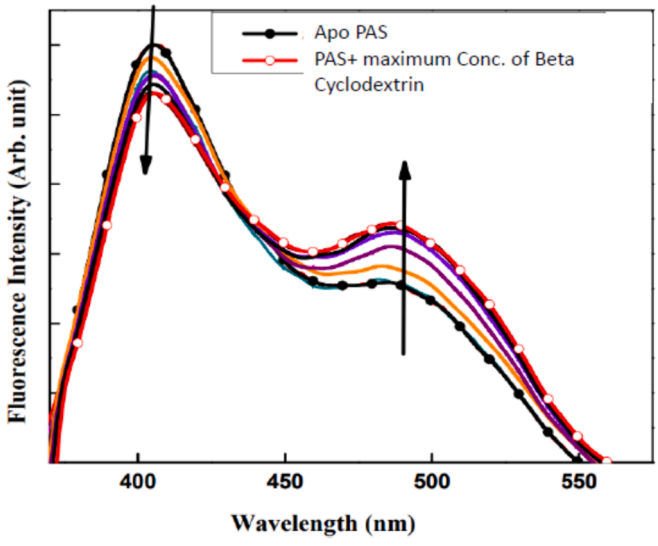

Fig. 7. Emission spectra of apo PAS, and PAS in presence of increasing β-CD concentration (10 mM to 20 mM).

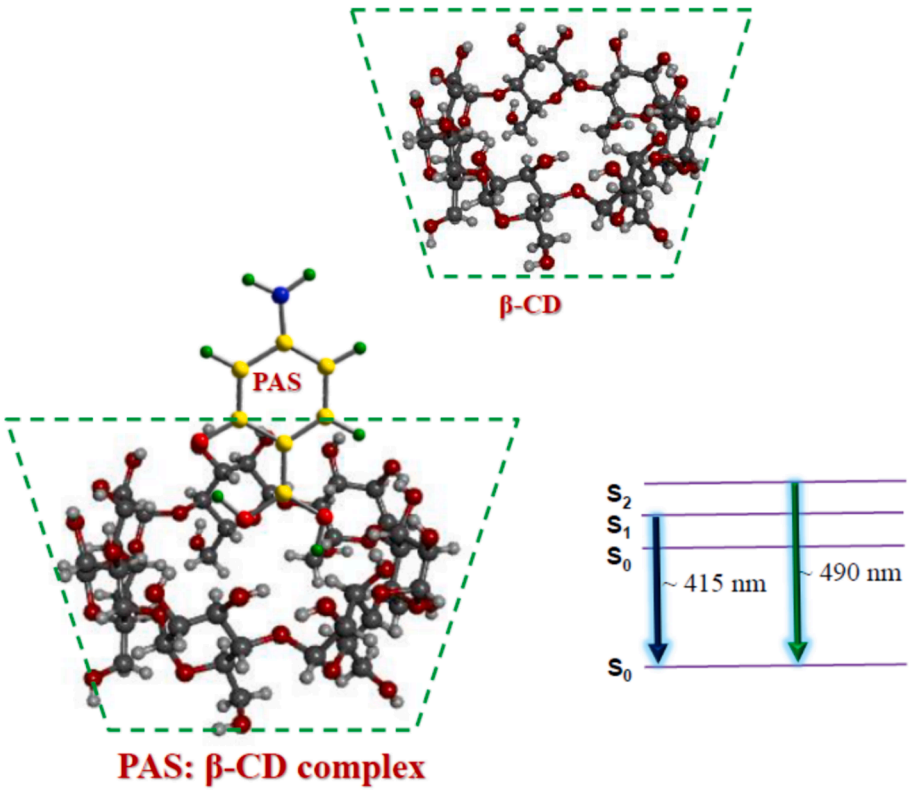

Fig. 8. Geometrical representation of β-CD and PAS: β-CD complex.

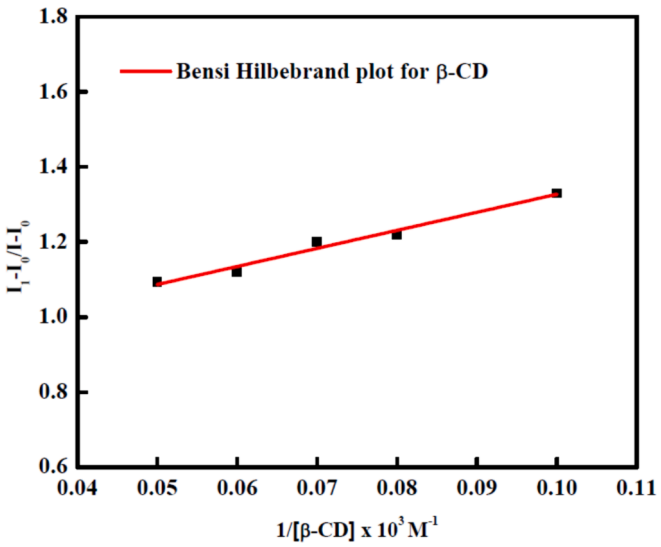

Fig. 9. Benesi-Hildebrand plot for PAS in presence of varying concentration of β-CD (10 mM to 20 mM).

300 K (room temperature). Number of hydrogen bonded and hydrophobic interactions always play a key role in identifying the inhibitor: receptor complexation [57] as larger the number is the measure of stability of energetically favoured ligand in a suitable pocket of the environment of receptor structure. In the present case, we have observed maximum number of conventional hydrogen bonds (hydrogen bonds between two atoms) for docked PAS: 3CGT complex structure in position 3. Hydrogen bonded interactions appeared between 3CGT (Residues: LYS47, HIS98, ARG375, ASP371) and PAS (atoms: O, H) (Fig. 10a-c, Table5, SD2). For the same pose maximum number of hydrophobic interactions were also observed between 3CGT (Residues: HIS98, TRP101) and PAS (Fig. 10, Table5). Lower value of dreiding energy (63.35) and binding energy (−5.1 kcal/mol) for pose 3 also validated the stronger interaction between PAS and 3CGT (SD2). All the above mentioned docking results clearly indicates that PAS can be easily bind inside the favorable pocket of receptor 3CGT and can form a stable PAS: 3CGT complex. To calculate inhibition constant, we have used the below mentioned equation:

$$K_i = e^{\Delta G/RT} \tag{12}$$

where the universal constant is R, the binding affinity is G, and the temperature is T (300 K). Lowest inhibition constant value (1.8×10^{-4} M) for pose 3 of PAS: 3CGT structure validated the stronger interaction of inhibitor PAS towards the receptor 3CGT.

3.8. Molecular dynamics (MD) simulation

In silico-based MD simulation approach can provide a detailed perspective in the growth of highly efficient mechanism of action for chemical leads for the development of drugs against various viral diseases [38,58]. Through molecular dynamics the most probable structure of the receptor: inhibitor (drug) inclusion complexes and their mechanism of interactions, stability of complex formation can be easily proposed. Simulated data can easily demonstrate whether the inhibitory effect of proposed drug can be retained after forming complexation with the receptor. For the present study, with the aim to understand the promising antitubercular activity of PAS, MD simulation was performed to support the mode of action, interaction and preferred active binding sites of the PAS: 3CGT complex. The MD simulation study of PSA: 3CGT complex structure along with bare 3CGT were performed for 50000 ps time scale. Through the use of numerous thermo dynamical parameters including RMSD, RMSF, and binding energy estimates, all the trajectories were examined in order to comprehend the stability and fluctuations of these complex structures. Before MD simulation, we have compared and analysed the minimum potential energy (E_{pot}) of

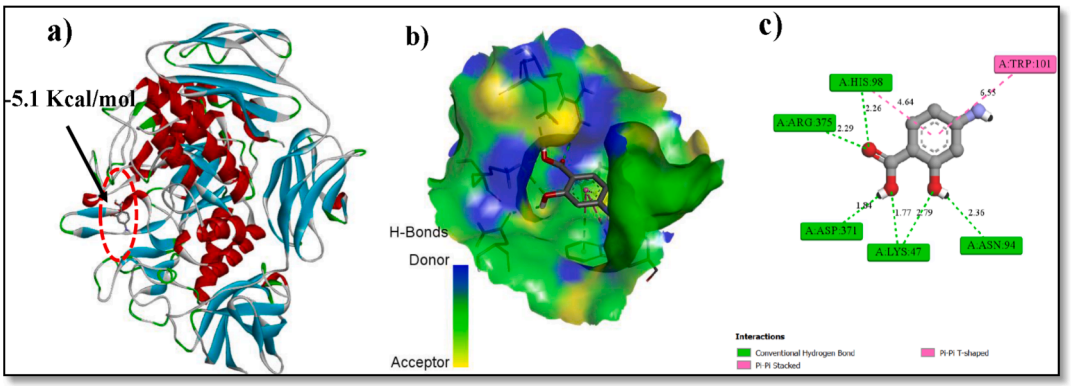

Fig. 10. a) binding energies pas, b) donor: acceptor surface for best pose in terms of h-bond interaction c) possible types of interaction in pose for pas: 3cgt.

Table 5
For the docked structure of PAS with receptor protein 3CGT, various interaction parameters.

Ligand	Binding affinity (kcal/mol)	Hydrogen bonded interaction (donor: acceptor, distance in \AA)[Type of bond]	Hydrophobic bonded interaction (donor: acceptor, distance in \AA) [Type of bond]	Dreiding energy (ligand)	Inhibition Constant (M) K_i=
PAS	−5.1	(A:LYS47:HZ2: PAS:O, 2.79) [Conventional Hydrogen Bond](A: LYS47:HZ2: PAS:O, 1.76) [Conventional Hydrogen Bond](A: HIS98:HD1: PAS:O, 2.25) [Conventional Hydrogen Bond](A: ARG375:HH21: PAS:O, 2.29) [Conventional Hydrogen Bond] (:PAS: H A: ASN94:OD1, 2.35) [Conventional Hydrogen Bond](:PAS: H A:ASP371: OD1, 1.84) [Conventional Hydrogen Bond]	(A:HIS98: PAS, 4.63) [Pi-Pi Stacked](A: TRP101: PAS, 5.25) [Pi-Pi T-shaped](A: TRP101: PAS, 5.02) [Pi-Pi T-shaped]	63.35	1.8×10^{-4}

Table 6
MD simulations results for receptor protein 3CGT in its apo state and for the PAS: 3CGT, complex structure.

S. No	Parameter	Apo protease (3CGT) Mean	Range	PAS: 3CGT Mean	Range
MD Simulation Result					
1.	**SR Columbic Interaction Energy (kcal/mol)**	NA	NA	−2.8	2.3- −6.4
2.	**SR LJ Interaction Energy (kcal/ mol)**	NA	NA	−21.9	−10.9- −28.2
3.	**RMSD (nm)**	0.35	0.15 – 0.5	0.165	0.05 – 0.35
4.	**Inter H-Bonds**	NA	NA	6	0–10
5.	**Radius of gyration (nm)**	2.6	2.5 – 2.61	2.53	2.48 – 2.56
6.	**SASA (nm^2)**	237.5	219—256	46	40—51
MM/PBSA Results					
7.	**Potential Energy (kcal/mol)**	-3.0×10^{-5}	NA	-2.5×10^{-5}	NA
10.	**Binding energy (ΔG) (kcal/mol)**	NA	NA	−19.96 0.09	NA
11.	**Van der Waal Energy (ΔE_{vdw}) (kcal/mol)**	NA	NA	–23.020.07	NA
12.	**Electrostatic Energy (ΔE_{elec}) (kcal/mol)**	NA	NA	−3.90.03	NA

stabilised structures of bare 3CGT and PSA: 3CGT complex (SD 3a and Table 6). The average E_{pot} of bare 3CGT and for PSA: 3CGT complex were obtained at same order as -3.0×10^{-5} kcal/mol for PAS and -2.5×10^{-5} kcal/mol for PSA: 3CGT (SD 3a, Table 6). E_{pot} values of the same order justifies the better possibility of complexation between PSA and 3CGT. After reaching the minimized energy state, initial stabilities of each structure were verified in the situation of equilibrium (NVT and NPT) for essential parameters: Temperature (T), density (D), pressure (P), and volume (V) for 100 ps trajectory (SD 3b-d). After all above mentioned verification MD simulation was performed with fully equilibrated state upto the time scale of 50000 ps and several thermo dynamical parameters were obtained for both apo 3CGT and PSA: 3CGT complex.

Drug specificity, such as metabolization, and complex stabilisation are studied from the interaction involving hydrogen bonds between a drug and a receptor [59]. From the MD simulation result (Fig. 11 and Table 5,6) it can be observed that PAS: 3CGT complex structure has six intermolecular hydrogen bonds which validated the molecular docking result. Larger number of H-bonded interaction justifies better stability of complex structure. Similarly Radius of gyration (R_g) of a complex structure with respect to the backbone receptor reflects its compactness [60]. Smaller the difference from reference structure better is the possibility of compactness of complex structure. The average R_g for the apo 3CGT backbone was obtained as 2.6 nm within the range of 2.5 – 2.61 nm whereas for PAS: 3CGT it was 2.53 nm within a range of 2.48 – 2.56 nm (Fig. 12). Perfect similarity of PAS: 3CGT with respect to its backbone validated the compactness of PAS: 3CGT structure.

RMSD is a parameter that is used to assess the stability of an inhibitor and its conformational deviation with respect to receptor backbone of receptor during simulation process [61]. RMSD analysis revealed that PAS: 3CGT complex is stable across the 50000 ps simulation period with an average value of 0.25 nm with respect to the reference 3CGT backbone having an average value of 0.35 nm (Fig. 13, Table 6). Low

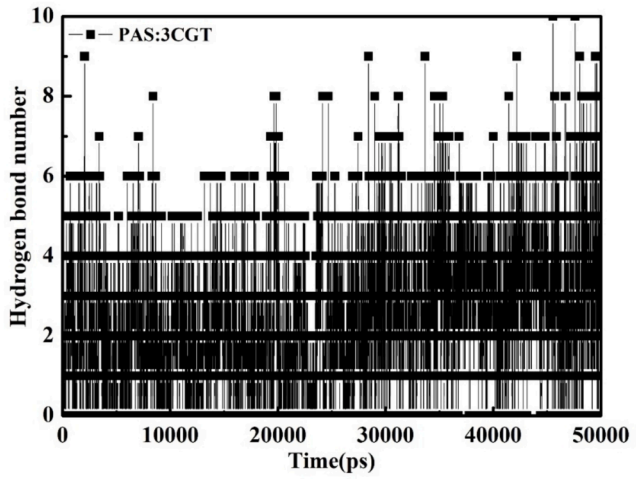

Fig.11. Intermolecular H-bond counts for the protein–ligand complex between PAS and 3CGT for different time points, from 0 ps to 50000 ps.

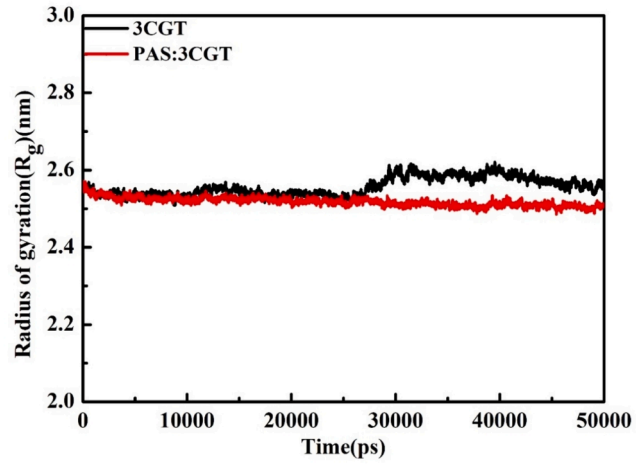

Fig. 12. For time trajectories from 0 ps to 50000 ps, the total radial gyration for apo 3CGT and the PAS: 3CGT complex.

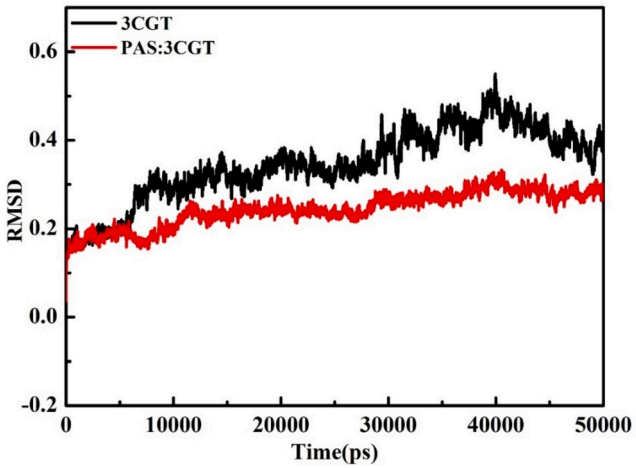

Fig. 13. RMSD (Root Mean Square Deviation) plots for receptor protein in the apo state 3CGT and in complex (PAS: 3CGT) with receptor protein 6LU7 up to 50000 ps.

fluctuation and lower values of RMSD are very good in sign in terms of system's stability [62]. RMSF is also used to examine the residue-by-residue fluctuations in PAS: 3CGT complex. RMSF identifies a receptor's flexible area and examines the parts of structure that vary in relation to the overall structure. A larger value of RMSF indicates the more flexibility throughout the MD simulation, whereas a lower RMSF value shows strong system stability. The average RMSF values for apo 3CGT, and PAS: 3CGT complex were noted as 0.12 and 0.10 respectively (Fig. 14, Table 6). To quantify the strength of the non-bonded interactions between PSA and 3CGT, we have computed the nonbonded interaction energies (Coulombic and Lenard Jones) between them. With the aid of colour contour depiction, Fig. 15a,b shows the variation of Coulombic interaction energy and Lenard Jones interaction energy with regard to time. Columbic interaction energy for the PAS: 3CGT complex is observed as −2.8 kcal/mol while Lennard-Jones interaction energy is −21.9 kcal/mol (Table 6). Above results conclude that during the complex formation, the Lennard-Jones interaction energy had a greater influence than the Coulombic interaction.

Further to scrutinize the binding affinity and key interactions between the guest PSA and 3CGT as receptor/ target for the inhibitor PSA, binding energy of PSA: 3CGT complex has been computed in fully equilibrated state by using MMPBSA method for the time scale of 50000 ps. MMPBSA is an efficient free energy simulation method to model molecular recognition. By MMPBSA method, binding energy of the inhibitor: receptor interactions have been computed by using equations (1–4) by calculating Van der Waal energy (E_{vdw}) and electrostatic energy ($E_{electrostatic}$) represented in Table 6. For best binding pose 3 of PAS: 3CGT has shown the best inhibitor to receptor binding affinity with the value of E_{vdw} as –23.020.07 kcal/mol and $E_{electrostatic}$ as −3.90.03 kcal/mol (Table 6, Fig. 16). The binding energy value for the PAS: 3CGT was obtained as −19.96 0.09 kcal/mol.

To check the stages of binding affinity of PAS towards 3CGT, the structural positions of PAS inside 3CGT have been studied for variable time trajectories from initial time (0 ps) and final (50000 ps) time frames (Fig. 17a). Fig. 17b represents the superposition of both binding phases. It is observed that PAS was initially outside of the binding site (green, 0 ps), but by the end of the simulation, it had moved closer to the binding cavity, with a little rotation and change in the functional group's position (red, 50000 ps). The initial and final frames of the ligand-bound receptor's perfect structural superimposition show very little change at the ligand binding region (Fig. 17 b). Only the ligand orientation has been changed throughout simulation for maximal convergence. Additionally, a slight tilt in the ligand position during simulation implies that PAS was properly bound at the 3CGT binding site (Fig. 17).

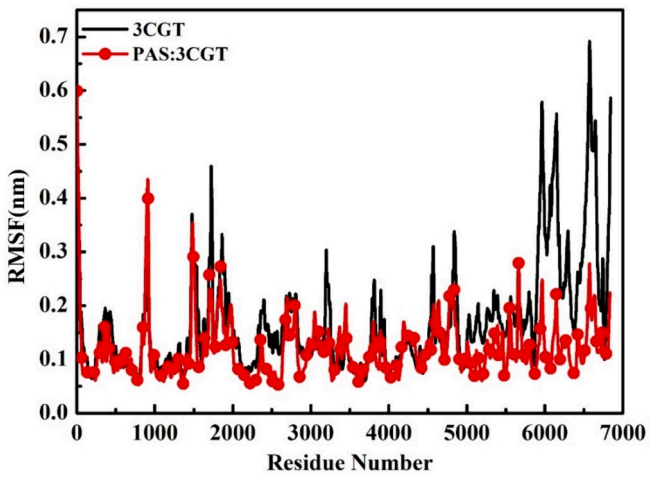

Fig. 14. Root mean square fluctuation (RMSF) graphs for apo state of receptor protein 3CGT and in complex (PAS: 3CGT) with receptor protein 3CGT up to 50000 ps.

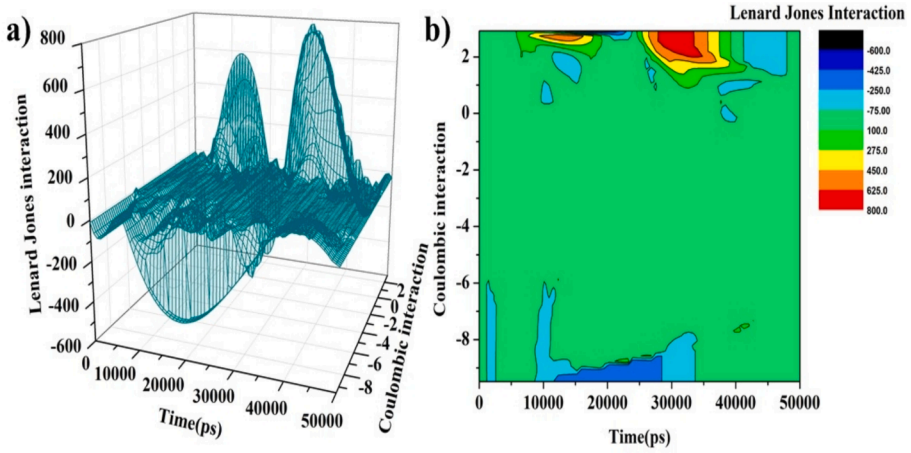

Fig. 15. For PAS: 3CGT complex: a)Variation of Coulombic interaction energy and Lenard Jones interaction energy with respect to time b) attached with color contour representation with specific color coding.

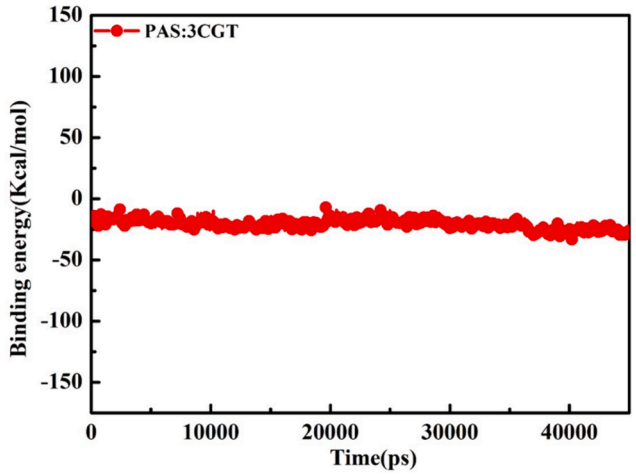

Fig. 16. Binding energy graph for PAS: 3CGT complex structure in time trajectory 0 ps to 50000 ps.

3.9. Principal component analysis and free energy landscape

We have employed principal component analysis (PCA) to determine the collective motion of the apo 3CGT and bound ligand with receptor 3CGT. PCA is employed to gain a deeper comprehension of the structural and conformational alterations in protein brought on by the binding of an inhibitor to a receptor. The eigenvectors (overall direction of motion of the atoms) and eigenvalues of the receptor's C_α atom are used in the PCA investigation (atomic contribution of motion) [63]. Analyzing conformational sampling of systems also involves tracing the covariance matrix for backbone atom locations. In the present paper, we have also computed the covariance trace value. For the apo 3CGT's covariance trace value was found to be 21.8 nm^2, while the PAS: 3CGT complex had a lower covariance trace value of 17.9 nm^2. Overall, PCA analysis demonstrated that binding of pas to 3CGT resulted in a significant shift in the overall motion of 3CGT, indicating that the conformational space of 3CGT is compressed (Fig. 18 (a–c)).

Fig. 19 (a,b) shows the energy minima landscape of unbound 3CGT and PSA: 3CGT complex with the free energy landscape (FEL) is compared to the first principal components PC (RMSD). For both examples, ΔG ranges from 2 to 10 kcal/mol (Fig. 19). The apo 3CGT and PAS: 3CGT complex's stability is indicated by the minimal variation of energy area and size.

4. Conclusion

Salicylic acid derivatives are probably best known for their diverse pharmacological properties. Some of the most important biological activities of salicylic acid derivatives include anti colitis, anti-ulcer etc activities. Among all salicylic acid derivatives, PAS has been attracted too much attention for its effective anti-tuberculosis activities. For this work, our initial step was to research the detailed structural parameters of PAS theoretically. We have observed PAS shows quite large variation of charge and dipole moment in its stable configuration. The high charge variation between its two charged moieties creates the reactiveness and the possibility of charge transfer of PAS towards its neighbouring environment. The chemical reactiveness of the ligand drug PAS was verified by using FMO parameters and HOMO to LUMO charge transfer. The possibility of charge transfer was further confirmed by contribution of lone pairs and π bonds in UV–vis spectra. All of the above mentioned factors suggested the PAS's reactivity, and thus its potential ability to bind to neighbouring environment for present case as drug carrier target receptor β-CD. Luminescence, molecular docking and MD simulation studies have revealed the stronger binding for PAS towards raw cyclodextrin glycosyltransferase enzyme and its product derivative β-CD. High value of association constant (K) 4.8 x 10^3 M^{-1} in aqueous environment validated the1:1 inclusion complex between PAS: β-CD. Similarly, high binding affinity (−5.1 Kcal/mol), a low inhibition constant (1.8×10^{-4}), presence of maximum number of non-bonded interactions including several other thermodynamic parameters like E_{pot}, RMSD, RMSF, R_g, SASA energy, interaction energies, ΔG_{bind} have also established the strong binding between PAS and 3CGT. Exact matching of number of hydrogen bonded interactions of PAS: 3CGT complex from molecular docking and MD simulation data validate the existence of strong binding force of the 1:1 PAS: 3CGT complex formation. Perfect resemblance of RMSD and RMSF values of PAS: 3CGT complex and apo 3CGT demonstrated the suggested drug's entire inheritance inside receptor site. We hope that the chemical reactivity of PAS presented in present work is expected to be relevant in TB drug discovery and development. The present in-silico and experimental research output on the drug PAS as an inhibitor towards nano-sized capping reagent β-CD as drug carrier will help researchers to characterise the "Green" behaviour of probe drug molecule in the nano dimensional binding region of target receptors including their whole biological processes.

CRediT authorship contribution statement

Shruti Sharma: Writing – review & editing, Writing – original draft, Investigation, Formal analysis, Data curation. **Pooja Yadav:** Writing –

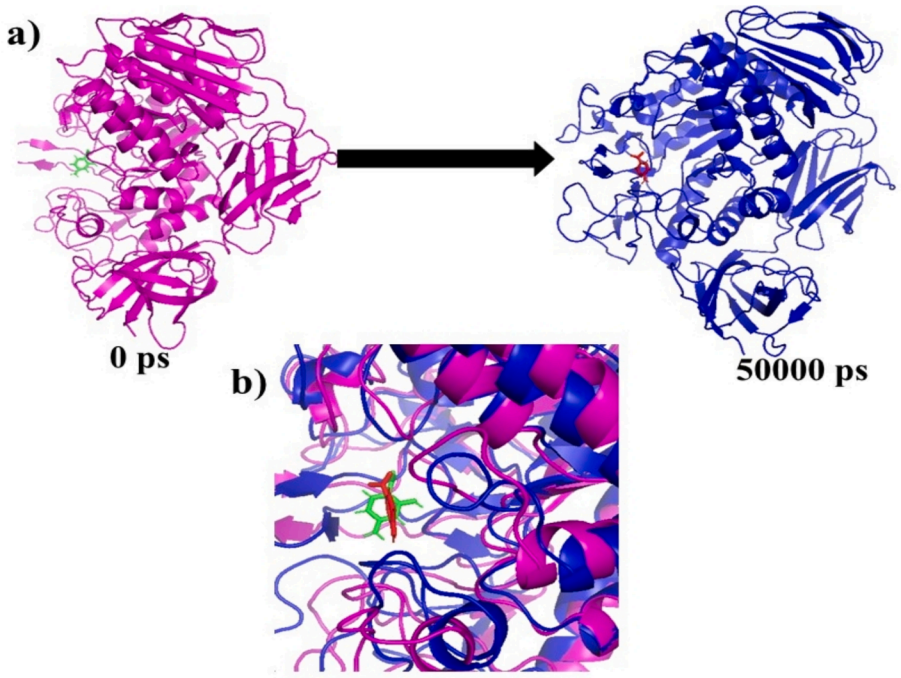

Fig. 17. a) structural position of first frame (0 ps) and last frame (50000 ps), b) Superposition of initial and final of F bound 3CLpro complex after MD simulation.

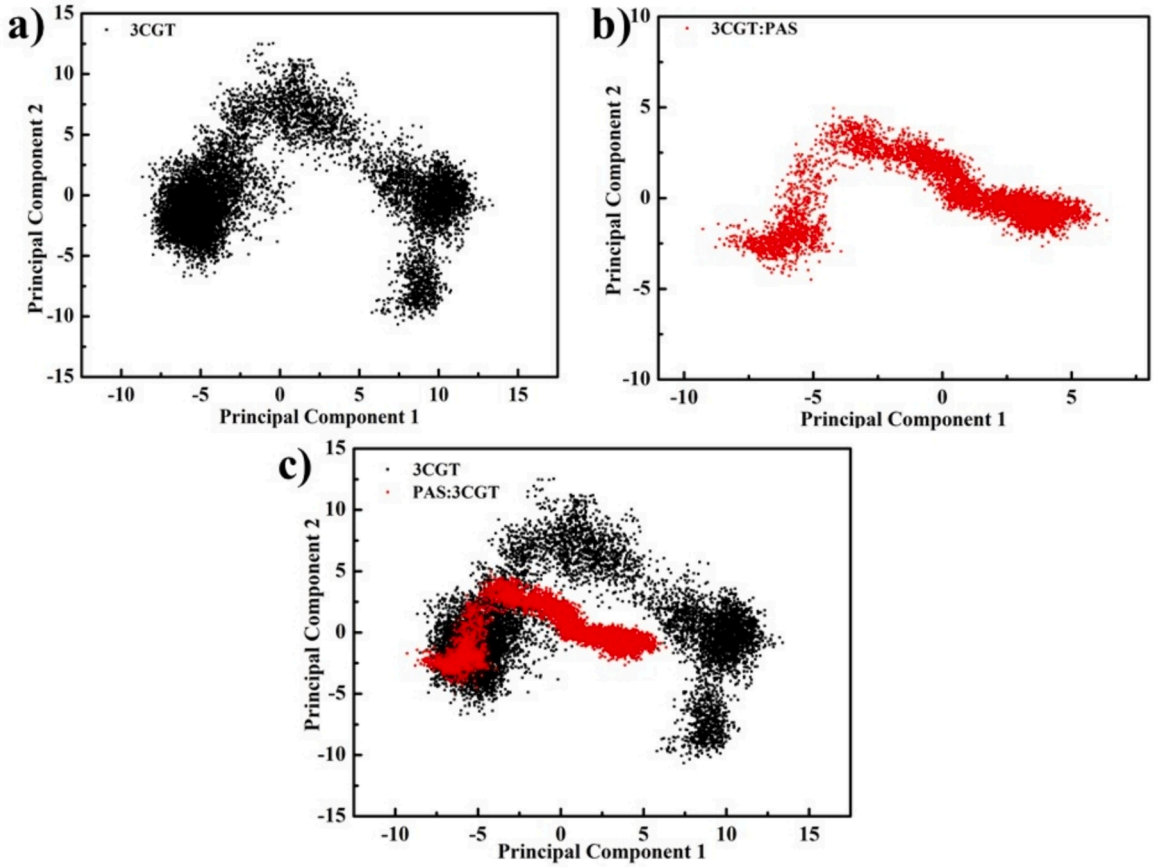

Fig. 18. Projection of β-CD phase space atoms along the first two major eigenvectors. (a) 3CGT (b) PSA: β-CD complex (c) Superimposed plot showing 3CGT unbound and PSA: 3CGT.

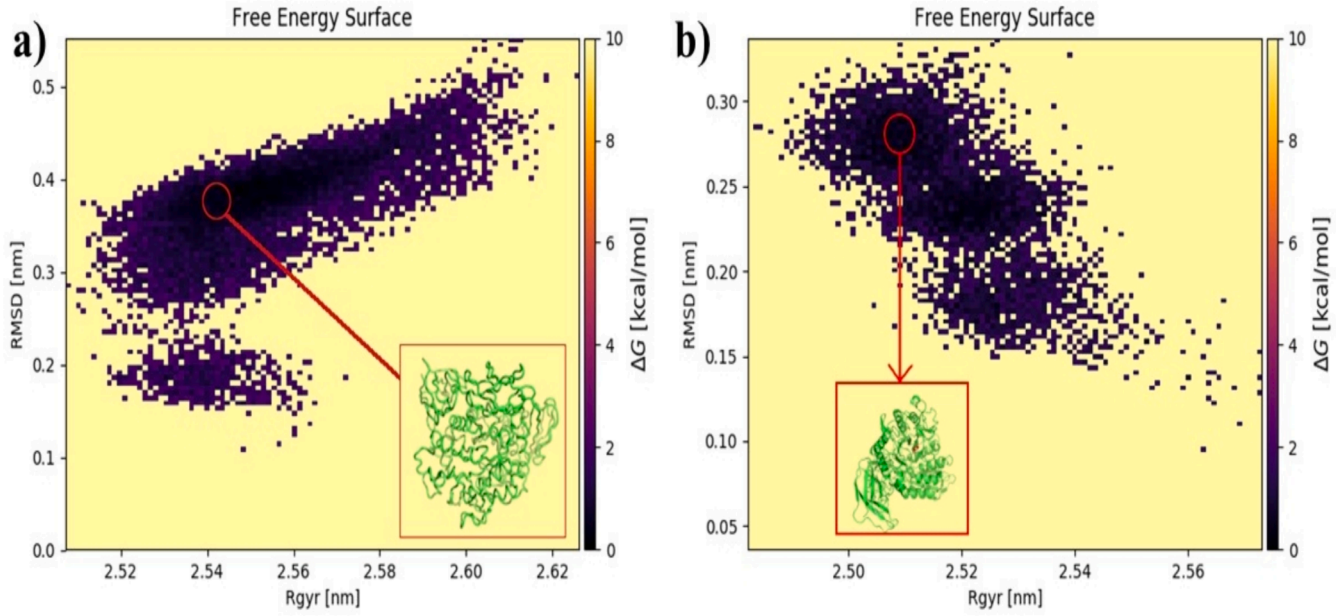

Fig. 19. Free energy landscape of the first principal components for (a) apo 3CGT (b) PSA: β-CD complex with standard inhibitor PAS.

original draft, Validation, Software, Investigation, Formal analysis, Data curation, Conceptualization. **Meenakshi Rana:** Writing – original draft, Validation, Software, Investigation, Conceptualization. **Papia Chowdhury:** Writing – review & editing, Validation, Supervision, Software, Methodology, Formal analysis, Conceptualization.

Declaration of competing interest

The authors declare that they have no known competing financial interests or personal relationships that could have appeared to influence the work reported in this paper.

Data availability

Data will be made available on request.

Appendix A. Supplementary data

Supplementary data to this article can be found online at https://doi.org/10.1016/j.molliq.2024.125611.

References

[1] A. Cohen, V.D. Mathiasen, T. Schön, C. Wejse, The global prevalence of latent tuberculosis: a systematic review and meta-analysis, Eur. Respir. J. 54 (3) (2019).
[2] Q. Liu, D. Yang, W. Xu, J. Wang, B. Lv, Y. Shao, H. Song, G. Li, H. Dong, K. Wan, Molecular typing of Mycobacterium tuberculosis isolates circulating in Jiangsu province, China, BMC Infect. Dis. 11 (1) (2011) 1–10.
[3] S. Gatadi, S. Nanduri, New potential drug leads against MDR-MTB: A short review, Bioorg. Chem. 95 (2020) 103534.
[4] S. Tiberi, G.B. Migliori, J.M. Chakaya, T. Kaesava, S.S. Al Abri, C. Wejse, D. Goletti, N. Kapata, G. Sotgiu, J. Bomanji, Commemorating World TB Day 2020:"IT'S TIME"—It's time to End the Global TB Epidemic, International Journal of Infectious Diseases 92 (2020) S1-S4.
[5] R. Liu, K. Marshall, R. Ma, K.L.T. Pham, G. Shetye, Z. Liu, S. Cho, H. Jeong, S. G. Franzblau, G.C. Moraski, Syntheses and studies of deuterated Imdiazo [1, 2-a] pyridine-3-carboxamides with potent anti-tuberculosis activity and improved metabolic properties, Bioorg. Chem. 128 (2022) 106074.
[6] Z. Ahsan Karar, N. Alam, P. Kim Streatfield, Epidemiological transition in rural Bangladesh, 1986–2006, Glob. Health Action 2 (1) (2009), 1904.
[7] Z. Zou, G. Liu, S.I. Hay, S. Basu, U.I. Belgaumi, A. Dhali, S. Dhingra, G. Fekadu, M. Golechha, N. Joseph, Time trends in tuberculosis mortality across the BRICS: an age-period-cohort analysis for the GBD 2019, EClinicalMedicine 53 (2022).
[8] J.F. Murray, A century of tuberculosis, Am. J. Respir. Crit. Care Med. 169 (11) (2004) 1181–1186.
[9] M. Moosazade, M. Jamshidi, M. Amiresmaili, A. Nezammahalleh, A comparison of directly observed therapy and self-administered therapy strategies in treatment of pulmonary tuberculosis: A cohort study in north of Iran, Middle-East J. Sci. Res. 11 (7) (2012) 873–880.
[10] R. Prasad, N. Gupta, A. Banka, Multidrug-resistant tuberculosis/rifampicin-resistant tuberculosis: Principles of management, Lung India: Official Organ of Indian Chest Society 35 (1) (2018) 78.
[11] P.E. Alexander, P. De, The emergence of extensively drug-resistant tuberculosis (TB): TB/HIV coinfection, multidrug-resistant TB and the resulting public health threat from extensively drug-resistant TB, globally and in Canada, Can. J. Infect. Dis. Med. Microbiol. 18 (2007) 289–291.
[12] S. Tiberi, R. Buchanan, J.A. Caminero, R. Centis, M.A. Arbex, M. Salazar, J. Potter, G.B. Migliori, The challenge of the new tuberculosis drugs, Presse Med. 46 (2) (2017) e41–e51.
[13] J. Stec, O.K. Onajole, S. Lun, H. Guo, B. Merenbloom, G. Vistoli, W.R. Bishai, A. P. Kozikowski, Indole-2-carboxamide-based MmpL3 inhibitors show exceptional antitubercular activity in an animal model of tuberculosis infection, J. Med. Chem. 59 (13) (2016) 6232–6247.
[14] D. Tenero, G. Derimanov, A. Carlton, J. Tonkyn, M. Davies, S. Cozens, S. Gresham, A. Gaudion, A. Puri, M. Muliaditan, First-time-in-human study and prediction of early bactericidal activity for GSK3036656, a potent leucyl-tRNA synthetase inhibitor for tuberculosis treatment, Antimicrobial agents and chemotherapy 63(8) (2019) 10.1128/aac. 00240-19.
[15] A.H. Diacon, A. Pym, M. Grobusch, R. Patientia, R. Rustomjee, L. Page-Shipp, C. Pistorius, R. Krause, M. Bogoshi, G. Churchyard, The diarylquinoline TMC207 for multidrug-resistant tuberculosis, N. Engl. J. Med. 360 (23) (2009) 2397–2405.
[16] Y. Lu, M. Zheng, B. Wang, L. Fu, W. Zhao, P. Li, J. Xu, H. Zhu, H. Jin, D. Yin, Clofazimine analogs with efficacy against experimental tuberculosis and reduced potential for accumulation, Antimicrob. Agents Chemother. 55 (11) (2011) 5185–5193.
[17] W.W.M. Formulary, Stuart, MC, Kouimtzi, M., Hill, SR, Eds, World Health Organization: Geneva, Switzerland (2009).
[18] J. Lehmann, Para-aminosalicylic acid in the treatment of tuberculosis, Lancet (1946) 15–16.
[19] J. Lehmann, Chemotherapy of Tuberculosis. The Bacteriostatic Action of P-Aminosalicylic Acid (PAS) and Closely Related Compounds Upon the Tubercle Bacillus, Together with Animal Experiments and Clinical Trials with PAS, Svenska Lakartidningen 43 (1946) 2029.
[20] J. Lehmann, The treatment of tuberculosis in Sweden with para-aminosalicylic acid (PAS): A review, Dis. Chest 16 (6) (1949) 684–703.
[21] F. Ryan, Tuberculosis: the greatest story never told: the human story of the search for the cure for tuberculosis and the new global threat, FPR-Books Ltd, 1992.
[22] H. Niyazi, Investigating the response of Mycobacterium tuberculosis to anti-tuberculosis drugs, UCL (University College London), 2021.
[23] C.A. Peloquin, Therapeutic drug monitoring in the treatment of tuberculosis, Drugs 62 (2002) 2169–2183.
[24] T. Törün, G. Güngör, I. Özmen, Y. Bölükbaşı, E. Maden, B. Bıçakçı, G. Ataç, T. Sevim, K. Tahaoğlu, Side effects associated with the treatment of multidrug-resistant tuberculosis, Int. J. Tuberc. Lung Dis. 9 (12) (2005) 1373–1377.
[25] C.-Y. Chiang, Integration of tuberculosis Services in Taiwan, 2001: challenges and opportunities, (2012).
[26] C. Peloquin, Pharmacometrics and tuberculosis, Springer, 2014.

[27] M. Rana, N. Singla, A. Chatterjee, A. Shukla, P. Chowdhury, Investigation of nonlinear optical (NLO) properties by charge transfer contributions of amine functionalized tetraphenylethylene, Opt. Mater. 62 (2016) 80–89.
[28] S. Lakhera, K. Devlal, M. Rana, I. Celik, Study of nonlinear optical responses of phytochemicals of Clitoria ternatea by quantum mechanical approach and investigation of their anti-Alzheimer activity with in silico approach, Struct. Chem. 34 (2) (2023) 439–454.
[29] A. Machelart, G. Salzano, X. Li, A. Demars, A.-S. Debrie, M. Menendez-Miranda, E. Pancani, S. Jouny, E. Hoffmann, N. Deboosere, Intrinsic antibacterial activity of nanoparticles made of β-cyclodextrins potentiates their effect as drug nanocarriers against tuberculosis, ACS Nano 13 (4) (2019) 3992–4007.
[30] M.H. Dahanayake, A.C. Jayasundera, Nano-based drug delivery optimization for tuberculosis treatment: A review, J. Microbiol. Methods 181 (2021) 106127.
[31] R.S. Kalhapure, N. Suleman, C. Mocktar, N. Seedat, T. Govender, Nanoengineered drug delivery systems for enhancing antibiotic therapy, J. Pharm. Sci. 104 (3) (2015) 872–905.
[32] V.J. Stella, Q. He, Cyclodextrins, Toxicologic Pathology 36 (1) (2008) 30–42.
[33] F. Tewes, J. Brillault, W. Couet, J.-C. Olivier, Formulation of rifampicin–cyclodextrin complexes for lung nebulization, J. Control. Release 129 (2) (2008) 93–99.
[34] D. Gugulothu, D.K. Khatri, Emerging applications of bionanomaterials in medicine and drug delivery, Emerging Applications of Bionanomaterials, Bionanotechnology, 2022, pp. 129–185.
[35] G.F.d.S. Fernandes, H.R.N. Salgado, J.L.d. Santos, Isoniazid: a review of characteristics, properties and analytical methods, Critical reviews in analytical chemistry 47(4) (2017) 298-308.
[36] K. Fathe, S. Ferrati, D. Moraga-Espinoza, A. Yazdi, H.D.C. Smyth, Inhaled biologics: from preclinical to product approval, Curr. Pharm. Des. 22 (17) (2016) 2501–2521.
[37] K.J. Seung, S. Keshavjee, M.L. Rich, Multidrug-resistant tuberculosis and extensively drug-resistant tuberculosis, Cold Spring Harb. Perspect. Med. 5 (9) (2015).
[38] P. Chowdhury, In silico investigation of phytoconstituents from Indian medicinal herb 'Tinospora cordifolia (giloy)'against SARS-CoV-2 (COVID-19) by molecular dynamics approach, J. Biomol. Struct. Dyn. 39 (17) (2021) 6792–6809.
[39] F. Cheng, W. Li, Y. Zhou, J. Shen, Z. Wu, G. Liu, P.W. Lee, Y. Tang, AdmetSAR: a comprehensive source and free tool for assessment of chemical ADMET properties, ACS Publications (2012).
[40] O. Trott, A.J. Olson, AutoDock Vina: improving the speed and accuracy of docking with a new scoring function, efficient optimization, and multithreading, J. Comput. Chem. 31 (2) (2010) 455–461.
[41] R. Dennington, T. Keith, J. Millam, GaussView, Version 4.1. 2, Semichem Inc., Shawnee Mission, KS (2007).
[42] M.J. Frisch, gaussian09, http://www. gaussian. com/ (2009).
[43] K. Raghavachari, Perspective on "Density functional thermochemistry. III. The role of exact exchange" Becke AD (1993) J Chem Phys 98: 5648–52, Theoretical Chemistry Accounts 103 (2000) 361-363.
[44] A.D. Becke, Density-functional thermochemistry. V. Systematic optimization of exchange-correlation functionals, J. Chem. Phys. 107 (20) (1997) 8554–8560.
[45] T. Koopmans, Ordering of wave functions and eigenenergies to the individual electrons of an atom, Physica 1 (1933) 104–113.
[46] H.J. Berendsen, D. van der Spoel, R. van Drunen, GROMACS: A message-passing parallel molecular dynamics implementation, Comput. Phys. Commun. 91 (1–3) (1995) 43–56.
[47] W.F. van Gunsteren, S. Billeter, A. Eising, P. Hünenberger, P. Krüger, A. Mark, W. Scott, I. Tironi, Biomolecular simulation: the GROMOS96 manual and user guide, Vdf Hochschulverlag AG an Der ETH Zürich, Zürich 86 (1996) 1–1044.
[48] R. Kumari, R. Kumar, O.S.D.D. Consortium, A. Lynn, g_mmpbsa- A GROMACS tool for high-throughput MM-PBSA calculations, Journal of chemical information and modeling 54(7) (2014) 1951-1962.
[49] A. Das, A. Das, B.K. Banik, Influence of dipole moments on the medicinal activities of diverse organic compounds, J. Indian Chem. Soc. 98 (2) (2021) 100005.
[50] P. Yadav, M. Rana, P. Chowdhury, DFT and MD simulation investigation of favipiravir as an emerging antiviral option against viral protease (3CLpro) of SARS-CoV-2, J. Mol. Struct. 1246 (2021) 131253.
[51] C.Y. Lee, C.N. Nanah, R.A. Held, A.R. Clark, U.G. Huynh, M.C. Maraskine, R. L. Uzarski, J. McCracken, A. Sharma, Effect of electron donating groups on polyphenol-based antioxidant dendrimers, Biochimie 111 (2015) 125–134.
[52] L.R. Domingo, M.J. Aurell, P. Pérez, R. Contreras, Quantitative characterization of the global electrophilicity power of common diene/dienophile pairs in Diels-Alder reactions, Tetrahedron 58 (22) (2002) 4417–4423.
[53] C.A. Lipinski, Lead-and drug-like compounds: the rule-of-five revolution, Drug Discov. Today Technol. 1 (4) (2004) 337–341.
[54] M. Zakerhamidi, M. Keshavarz, H. Tajalli, A. Ghanadzadeh, S. Ahmadi, M. Moghadam, S. Hosseini, V. Hooshangi, Isotropic and anisotropic environment effects on the UV/vis absorption spectra of three disperse azo dyes, J. Mol. Liq. 154 (2–3) (2010) 94–101.
[55] H.A. Benesi, J. Hildebrand, A spectrophotometric investigation of the interaction of iodine with aromatic hydrocarbons, J. Am. Chem. Soc. 71 (8) (1949) 2703–2707.
[56] S. Sharma, A. Sharma, U. Gupta, Molecular Docking studies on the Anti-fungal activity of Allium sativum (Garlic) against Mucormycosis (black fungus) by BIOVIA discovery studio visualizer 21.1. 0.0, (2021).
[57] R. Patil, S. Das, A. Stanley, L. Yadav, A. Sudhakar, A.K. Varma, Optimized hydrophobic interactions and hydrogen bonding at the target-ligand interface leads the pathways of drug-designing, PLoS One 5 (8) (2010) e12029.
[58] P. Yadav, P. Chowdhury, Effectivity of repurposed drugs against SARS-CoV-2 infections, A hope for COVID 19: inhibitor modelling studies by docking and molecular dynamics, Heliyon 8 (12) (2022).
[59] S.-L. Chen, H. Yu, H.-M. Luo, Q. Wu, C.-F. Li, A. Steinmetz, Conservation and sustainable use of medicinal plants: problems, progress, and prospects, Chin. Med. 11 (2016) 1–10.
[60] M. Nygaard, B.B. Kragelund, E. Papaleo, K. Lindorff-Larsen, An efficient method for estimating the hydrodynamic radius of disordered protein conformations, Biophys. J . 113 (3) (2017) 550–557.
[61] K. Sargsyan, C. Grauffel, C. Lim, How molecular size impacts RMSD applications in molecular dynamics simulations, J. Chem. Theory Comput. 13 (4) (2017) 1518–1524.
[62] A. Kuzmanic, B. Zagrovic, Determination of ensemble-average pairwise root mean-square deviation from experimental B-factors, Biophys. J . 98 (5) (2010) 861–871.
[63] C.R. Sahoo, S.K. Paidesetty, B. Dehury, R.N. Padhy, Molecular dynamics and computational study of Mannich-based coumarin derivatives: Potent tyrosine kinase inhibitor, J. Biomol. Struct. Dyn. 38 (18) (2020) 5419–5428.